

Article

Investigation of the Shear Mechanism at Sand-Concrete Interface under the Influence of the Concave Groove Angle of the Contact Surface

Zhigang Meng ¹, Yunsong Li ², Huanhuan Li ¹, Songlin Shen ³ and Haijiang Zhang ^{4,5,*}¹ School of Civil Engineering and Architecture, NingboTech University, Qianhu South Road, Ningbo 315100, China; nblg_tjxy_m@nbt.edu.cn (Z.M.); huanhuanli17@nbt.edu.cn (H.L.)² School of Civil Engineering, Anhui Jianzhu University, No. 292 Ziyun Road, Hefei 230601, China; lys@stu.ahjzu.edu.cn³ China MCC22 Group Corporation Ltd., 16 Xingfu Road, Tangshan 063000, China; shensonglin@22mcc.com.cn⁴ School of Civil Engineering, Shaoxing University, Shaoxing 312000, China⁵ Key Laboratory of Rock Mechanics and Geohazards of Zhejiang Province, Shaoxing 312000, China

* Correspondence: haijiang1086@usx.edu.cn

Abstract: A “random-type” sand–concrete interface shear test was developed based on the sand cone method, with a focus on the most commonly encountered triangular contact surface morphology. A “regular-type” triangular interface, matched in roughness to the “random-type”, was meticulously designed. This “regular-type” interface features five distinct triangular groove inclinations: 18°, 33°, 50°, 70°, and 90°. A series of sand–concrete interface direct shear tests were conducted under consistent compaction conditions to investigate the impact of varying compaction densities and triangular groove inclinations on the shear strength at the interface. Particle flow simulations were utilized to examine the morphology of the shear band and the characteristics of particle migration influenced by the triangular contact surface. This analysis is aimed at elucidating the influence of the inclination of the triangular groove on the shear failure mechanism at the sand–concrete interface. The findings indicate that: (1) The morphology of the interface significantly impacts the shear strength of the sand–concrete interface, while the shape of the stress-displacement curve experiences minimal alteration. (2) At smaller inclination angles, particle contact forces are arranged in a wave-like configuration around the sawtooth tip, resulting in a non-uniform stress distribution along the sawtooth slope. However, as the inclination angle grows, the stress concentration at the sawtooth tip diminishes, and the stress distribution across the sawtooth slope becomes more consistent. (3) Particle migration is significantly influenced by the sawtooth’s inclination angle. At lower angles, particles climb the structure’s tip through sliding and rolling. As the angle increases, particle motion shifts to shear, accompanied by a transition in friction from surface friction to internal shear friction. This leads to the formation of a wider shear band and an increase in shear strength.



Citation: Meng, Z.; Li, Y.; Li, H.; Shen, S.; Zhang, H. Investigation of the Shear Mechanism at Sand-Concrete Interface under the Influence of the Concave Groove Angle of the Contact Surface. *Buildings* **2024**, *14*, 1452. <https://doi.org/10.3390/buildings14051452>

Academic Editor: Sufen Dong

Received: 8 April 2024

Revised: 12 May 2024

Accepted: 13 May 2024

Published: 17 May 2024

Keywords: sand–concrete interface; shear strength; shear mechanism; interface morphology; particle migration



Copyright: © 2024 by the authors. Licensee MDPI, Basel, Switzerland. This article is an open access article distributed under the terms and conditions of the Creative Commons Attribution (CC BY) license (<https://creativecommons.org/licenses/by/4.0/>).

1. Introduction

In the realm of geotechnical engineering, the shear behavior of the sand–concrete interface has a profound impact on the distribution of stress and deformation within foundation structures. This, in turn, affects the stability and longevity of the entire construction; it constitutes a primary research focus within the field of geotechnical engineering [1–3]. During the interaction between soil and a structural entity, the various surface features of the structure—including its contours, the configuration and interweaving of textures, and the scale of these textures—directly influence the contact area between the soil and the structure, thereby affecting the shear mechanism. In the academic sphere, the term

“roughness” is frequently employed to characterize structural surfaces, which are typically classified into two categories: “regular-type” and “random-type”. Scholars have studied the excitation effect of structural textures, such as periodic rectangular surfaces, trapezoidal surfaces, triangular surfaces, wave textures, and snake textures on the interfacial shear strength through various types of interface shear experiments [4–6]. They have investigated the shear failure behavior of interfaces such as soil–concrete, soil–steel, soil–geosynthetic membrane, etc., [7–9]. The research indicates that the interface morphology is a key factor influencing the interfacial shear strength, whether it is cohesive soil or cohesionless soil [10,11]. This is of significant importance for the design and performance evaluation of the engineering structures.

In the study of shear characteristics at the soil–structure interface, such as pile foundations, retaining walls, and earth dams, when the contact surface between cohesive soil and concrete is smooth, the shear peak and residual shear strength are very close and there is no volume expansion. When the surface roughness increases, the shear strength also increases and shear expansion occurs [12–14]. In sandy materials, the interface morphology also directly affects the interfacial shear strength, with the maximum shear strength being excited by random rough surfaces, followed by triangular surfaces, while rectangular surfaces have the lowest strength. Among “regular” surfaces, when the ratio of the protrusion spacing to the average particle size is between 1.0 and 3.0 and the ratio of protrusion height to average particle size is greater than 0.9, the interfacial shear strength reaches its highest excitation values [15,16].

After validation through centrifugal pile load tests, the shear strength stimulated by the serpentine surface structure is directly related to the direction of shear [17]. When the direction of the shear is opposite to the serpentine pattern, there is a significant increase in shear resistance and volume expansion. Furthermore, when the scale height, scale length, and texture direction are appropriately arranged, the shear strength stimulated by the serpentine surface exceeds that of the random surfaces, resulting in more intense particle displacement and rotation.

In the physical experimental studies of the soil–structure interface, it has also been found that factors such as particle size, particle gradation, particle shape, particle fracture characteristics, and cyclic loading significantly affect the interfacial shear strength [10,18–20]. However, due to the complexity of particle characteristics, it is often difficult to obtain the particle movement within the interface region through physical direct shear tests, and it is not possible to reveal the formation and change mechanisms of interfacial shear strength from a microscopic perspective. Therefore, numerical simulation techniques are commonly used to study the interface shear mechanisms at smaller scales [21–23]. Among these, the three-dimensional Discrete Element Method (DEM) discretizes the soil body into a collection of individual particles, which is widely used in soil–structure contact problems [24,25]. Extensively validated, DEM simulations show material responses that are consistent with physical experimental results under various conditions.

In summary, researchers have made substantial progress in understanding the mechanical properties of soil–structure interfaces. However, the influence of the specific surface topography on the shear behavior at these interfaces remains an area for further investigation; in particular, a clearer elucidation of the mesoscale shear mechanisms of sand particles on structured surfaces is required. Addressing this gap, this study employs a sand-filling method to conduct shear tests on “random” concrete surfaces under conditions of equal roughness, simplifying local contact geometries to semi-circular, triangular, rectangular, and trapezoidal shapes, among others. Focusing on the most prevalent triangular pattern, the research identifies five “regular” triangular concrete interfaces based on the slant angle of the side of the triangle’s groove— 18° , 33° , 50° , 70° , and 90° . A series of direct shear tests were performed on sand–concrete interfaces at a constant relative density to examine the effect of the angle of the triangular groove on the shear stress-displacement relation. Employing particle flow simulations, this study analyzes the morphology of the shear band and the characteristics of particle migration under the influence of triangular contact

surfaces, thereby elucidating the role of varying triangular groove angles in the mechanism of shear failure in concrete surfaces.

2. Test Methods and Results

2.1. Test Equipment and Materials

The ZJ strain-controlled direct shear apparatus produced by Nanjing Soil Instrument Factory Co., Ltd. (Nanjing, China) was adopted for the direct shear tests. Natural stone sand and cement were used as test materials, and the grain distribution of the sand was measured based on a sieve method according to the Geotechnical Test Method Standard GBT 50123-2019 [26]. The minimum and maximum dry densities of the sand were measured based on the dry density test and used to calculate the relative compactness of the sand, whose specific property parameters are listed in Table 1. The physical characteristics of the sand samples, the CT cross-sectional tomography methods, the 3D-printing methods for concrete molds, and the direct shear test process have been discussed in the author's previous study [27]. In this study, a further discussion was conducted on the test results, with a focus on the study of shear mechanisms based on the Particle Flow Simulation Method.

Table 1. Physical property indicators of sandy soil.

G_s	e_{\max}	e_{\min}	d_{10} (mm)	d_{30} (mm)	d_{60} (mm)	C_u	C_c
2.65	1.04	0.57	0.30	0.61	1.39	4.63	0.89

2.2. Sample Preparation

By conducting mortar–concrete slurry diffusion tests, we obtained concrete specimens characterized by random surface topographies. Subsequently, employing CT sectional slicing technology, the specimens were scanned to generate tomographic images depicting the diffusion of the concrete slurry across various sections (refer to Figure 1), the boundary of mortar–concrete slurry is marked as red line, while the green part stands for its diffusion area.

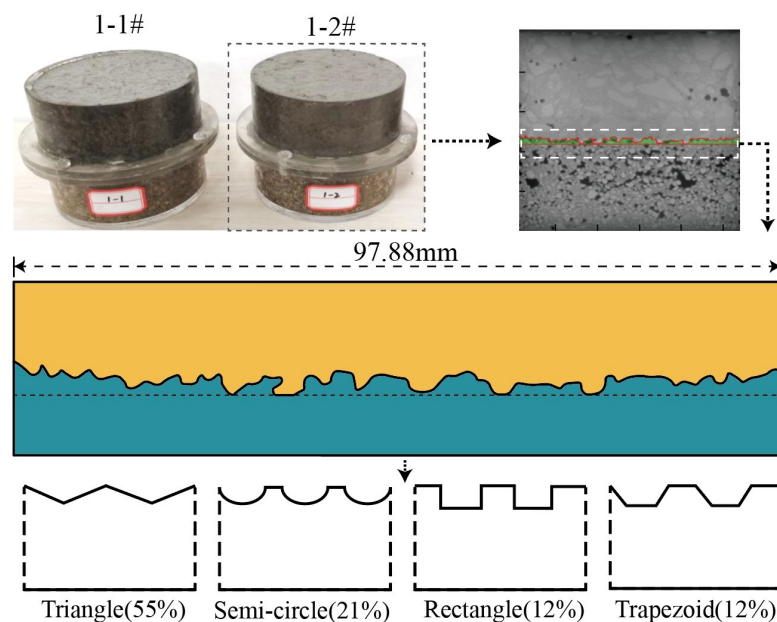


Figure 1. CT image of the slurry diffusion cross-section in the XZ direction of a sample. Adapted with permission from Ref. [27]. 2023, Huanhuan Li.

The morphology of the contact surface was examined, and random contact surfaces were generalized into triangles, semicircles, rectangles and trapezoids. Each shape had a

corresponding probability of occurrence: triangles at 55%, semicircles at 21%, rectangles at 12%, and trapezoids at 12%. Using the triangular contact, which is most frequently encountered, as a prototypical example, this study investigates the shear properties of triangular contact surfaces with jagged edges at various angles. The serration angle is determined by the size of the oblique angle along the side of the triangle's groove, angle values are set at 18° , 33° , 50° , 70° , and 90° , respectively, as depicted in Figure 2. The dimensions of the various sections are provided in Table 2. The random roughness of the concrete surface is typically assessed using the average depth of sand filling, which yields a roughness of 2.6 mm for the concrete's random surface morphology. To fabricate a triangular contact surface with the same roughness, the depth of the triangular groove was also adjusted to 2.6 mm.

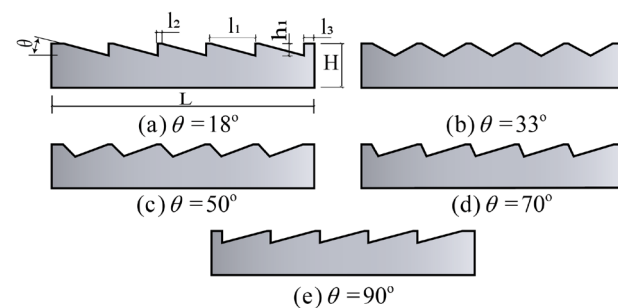


Figure 2. The feature of the triangular contact surfaces at different angles.

Table 2. Design parameters for the triangular contact surfaces at different angles.

Concrete Block	L (mm)	H (mm)	l_1 (mm)	l_2 (mm)	l_3 (mm)	h_1 (mm)
$\theta = 18^\circ$	96	20	17.14	0.72	3.71	5.46
$\theta = 33^\circ$	96	20	17.14	0.72	3.71	5.46
$\theta = 50^\circ$	96	20	17.14	0.72	3.71	5.46
$\theta = 70^\circ$	96	20	17.14	0.72	3.71	5.46
$\theta = 90^\circ$	96	20	17.14	0.72	3.71	5.46

2.3. Test Method and Result Analysis

In order to investigate the shear characteristics of sandy soil–structure contact interfaces with triangular configurations under varying triangle inclinations, a series of shear tests were conducted with four different normal stress conditions (50 kPa, 100 kPa, 200 kPa, and 300 kPa). Below the shear box, a square triangular profile of concrete with 96 mm sides was used. A cylindrical specimen of sandy soil, with a diameter of 61.8 mm and a height of 20 mm, was placed above the shear box. Five distinct concrete surface types were tested in conjunction with three relative soil densities ($Dr = 30\%$, 50% , and 70%) under the specified normal stresses, resulting in a comprehensive set of 18 test configurations. The sandy soil specimen was compressed against the triangular grooves in the concrete surface under normal stress application to create a sandy soil–structure contact interface. The shear test was performed at a constant shear rate of 1.2 mm/min and the shear stress-shear displacement relation is shown in Figure 3. Real-time data collection for direct shear testing was achieved using a dedicated geotechnical test data acquisition and processing system.

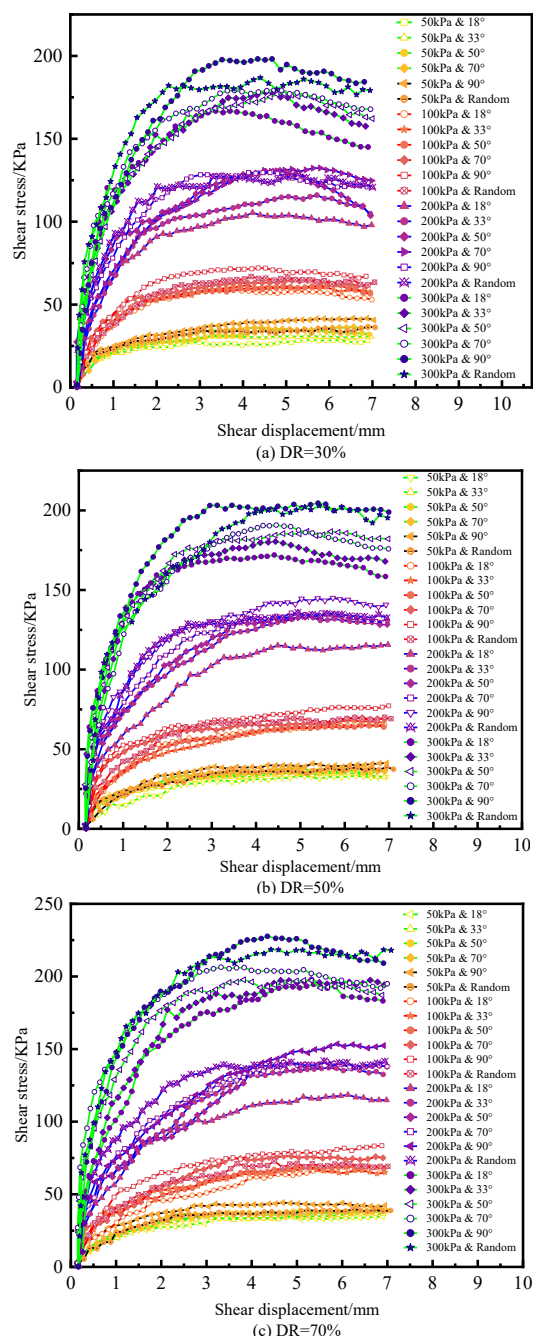


Figure 3. Shear stress-shear displacement relationship curve.

Figure 3 reveals that the shear stress-displacement curves at various densities follow a consistent pattern. At lower normal stresses (50 kPa and 100 kPa), the shear stress-shear displacement curves demonstrate ideal elastic-plastic behavior. Conversely, at higher normal stresses (200 kPa and 300 kPa), the curves exhibit a pronounced softening behavior. The shear stress-shear displacement curve for the original contact surface typically falls between the 70° and 90° triangle contact surfaces.

As the density of sandy soil undergoes alterations, the soil exhibits strain softening characteristics at lower initial relative densities ($Dr = 30\%$), progressing to strain hardening behaviors at higher relative densities ($Dr = 70\%$). This phenomenon has been attributed to an incremental densification process that induces compression and the closer packing of sand particles. Subsequently, the mechanical interlocking effect between the particles intensifies, culminating in an elevated shear resistance.

The magnitude of the friction coefficient enhancement ascribable to alterations in the sawtooth inclination angle exhibits variability across disparate intervals (Figure 4). Notably, within the specified ranges of 18° to 33° and 70° to 90° , a 1° increase in the inclination angle is correlated with a respective 3.7% increment in the friction coefficient. Conversely, when the angle spans between 33° to 70° , a 1° rise in the inclination angle elicits a 1.6% increase in the friction coefficient. Under the conditions of equivalent relative density, the friction angles of the interfaces are ranked from largest to smallest as follows: 90° interface > random interface > 70° interface > 50° interface > 30° interface > 18° interface.

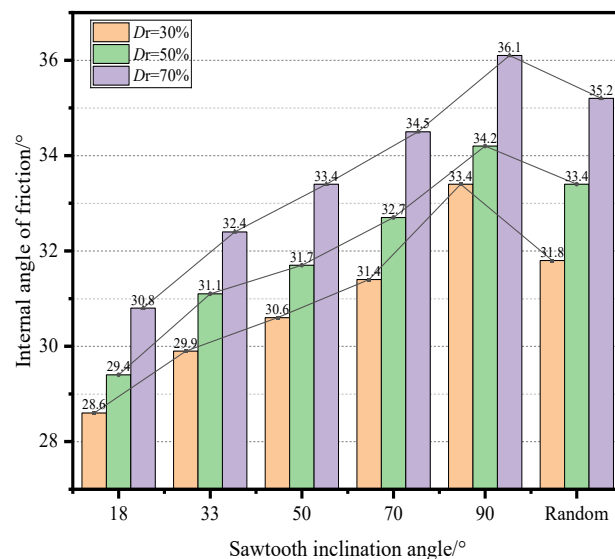


Figure 4. The impact of the relative compaction and serration angle on the internal angle of friction.

3. Numerical Simulation and Direct Shear Test Verification of Serrated Interface

3.1. Establishment and Parameter Determination of PFC Model

In the presence of “regular” sawtooth contact surfaces, the properties of particle shearing, and migration patterns significantly influence shear strength outcomes. The development of shear bands during the displacements of different contact surface types exhibits variations that are correlated with the characteristics of particle migration. The complexity of these dynamics makes it difficult to capture them through an indoor direct shear test due to the continuous changes in particle motion throughout the shear. The PFC program uses a particle flow analysis method based on the generic discrete element model (DEM) framework to simulate the motion and interaction of particles. Particles exert forces and torques on each other through internal inertia and moments, and their motion follows Newton’s laws of motion. The particles themselves are considered rigid bodies. This study is based on the PFC program for modeling analysis, and the particle grading and direct shear tests are consistent (Table 3). The particle contact model uses a linear model.

Table 3. Particle size range and volume fraction in the PFC2D.

Gravel Size	Volume Fraction
≤ 0.075 mm	1%
0.075 mm~0.25 mm	6%
0.25 mm~0.5 mm	15%
0.5 mm~1 mm	30%
1 mm~2 mm	20%
2 mm~5 mm	30%
≤ 0.075 mm	1%

To address this challenge, the PFC2D 6.0 particle flow software is employed in this study for modeling and analysis purposes. The upper and lower shear boxes, including the shear surfaces, were simulated utilizing a “generalized wall”, as illustrated in Figure 5, with the model dimensions specified as 61.8 mm × 4.0 mm (length × height). The upper shear boxes are identified by the markers ①②③, the obstructing structures by ④⑥, and the lower shear boxes by ⑦⑧⑨, while ⑩ denotes the unique shear surface configuration.

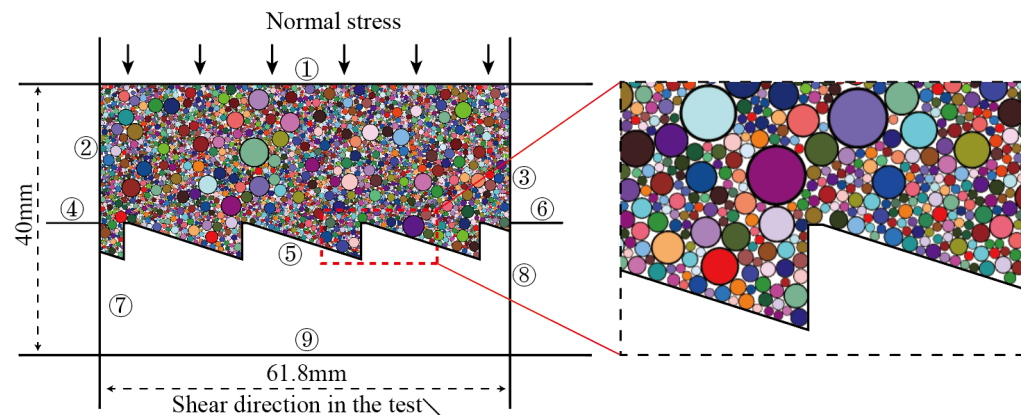


Figure 5. Numerical model of the direct shear for serrated contact surfaces.

In the course of the shearing experiment, elements ①②③⑥ are held stationary, while elements ④⑦⑧⑨⑩ are displaced to the right at a steady pace of 1.2 mm/min, thereby simulating the direct shear interaction between “sawtooth contact interfaces” and “sand particles”. The model assumes that the sand particles act as rigid spheres while maintaining a constant density of 2.0 g/cm³. For the duration of this study, the normal and tangential contact stiffnesses between the particles, as well as between the particles and the wall, are both set to 2×10^8 N/m. The number of particles in different models ranges from about 2500 to 2800. This study established six types of interfaces, each maintaining consistent particle size ranges and volume fractions used. Additionally, each model applied four types of normal stresses, specifically 50 kPa, 100 kPa, 200 kPa, and 300 kPa. The precise parameters of the model are provided in Table 4.

Table 4. Simulation parameters of the PFC2D.

Angle of the Contact Surface/(°)	Normal Stress (σ)/kPa	Interfacial Friction Coefficient (μ_i)	Particle Friction Coefficient (μ)
$\theta = 18^\circ$	50/100/200/300	0.32	0.91
$\theta = 33^\circ$	50/100/200/300	0.32	0.91
$\theta = 50^\circ$	50/100/200/300	0.32	0.91
$\theta = 70^\circ$	50/100/200/300	0.32	0.91
$\theta = 90^\circ$	50/100/200/300	0.32	0.91
Random	50/100/200/300	0.32	0.91

3.2. Simulation Result Analysis

The simulation results show that, within the same model, the characteristics of particle displacement and the development of inter-particle contact forces under different normal stresses are similar. For brevity, this study confines test conditions to a constant normal pressure of 200 kPa. This focus enables the exploration of the dynamics of particle contact force chains within the shear band and their correlation with particle displacement as shear displacement varies. As depicted in Figure 6, at an angle θ of 18° , the initial contact force chains are significantly influenced by the sawtooth geometry, forming an “arch” structure at the tips of the sawteeth. The force distribution on the zigzag surface is primarily concentrated at these cusps. As the shear displacement increases, the area occupied by the

arch between the teeth decreases. When the shear displacement exceeds 3 mm, the value of the force chain decreases in the central region of the shear surface, whereas the intensity of the force chain increases in the terminal region of the shear surface, creating arches across the zigzag. The angle of inclination of the force chain arch with respect to the horizontal is approximately 43°.

At an inclination angle (θ) of 33°, the formation of contact force chains is localized to the initial shear stage, with the subsequent dissipation of the arching effect as shear displacement augments. The distribution of contact forces across the zigzag surface is uniform and free of significant clustering in the force chain network. The direction of the force chain propagation is inclined at approximately 45° relative to the horizontal plane. For θ values of 50° or 70°, the phenomena of force chain arching and the uniform distribution of forces across the inclined sawtooth surface are observed concurrently. The localized arching effect is evident at the left end of the shear band, whereas the right end experiences a focal concentration of force along the zigzag edge. The tilt angle of the force chains is inclined at approximately 27°–29° with respect to the horizontal plane. At $\theta = 90^\circ$, the arching effect between the sawteeth is minimal, with the tilt direction of the force chains predominantly aligning with the orientation of the sawtooth slope. The contact force is primarily induced by the sawtooth surface, with an angle of tilt of approximately 21° relative to the horizontal plane. For random contact surfaces, the distribution of force chains is relatively homogeneous. The force chains arrange an arcuate configuration between the shear band and the right wall of the upper shear box, devoid of any internal arching structures within the shear band, with an angle of tilt of approximately 29° relative to the horizontal plane.

As illustrated in Figure 7, the vectorial representation of the particle displacement indicates that the maximum displacement is localized in the vicinity of the contact interface. The component of the particle displacement parallel to the shear direction is found to be consistent with the direction of propagation of the shear. Particles situated above the shear band exhibit a net upward migration, whereas those within the shear band exhibit displacement vectors that exhibit a “wavy” configuration. With an increase in the angle of inclination, the amplitude of the “waves” initially increases before decreasing. At an inclination angle of $\theta = 18^\circ$, particles adjacent to the vertical edge of the sawteeth exhibit the initial stages of loosening and displacement, whereas those proximate to the inclined edge of the sawteeth are propelled forward by the “wall” effect. Under other inclinations, the particle experiences displacement primarily due to the transverse pressure exerted by the inclined surface of the sawtooth. In contrast to the regular “wavy” displacement pattern induced by the geometrically shaped shear surface, the random shear surface generates a layer of irregular “waves” with varying thicknesses, with the amplitude of particle displacement being observed to increase in close proximity to the shear interface.

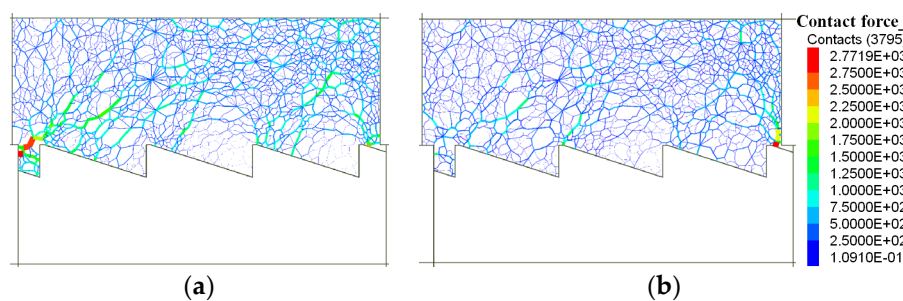


Figure 6. Cont.

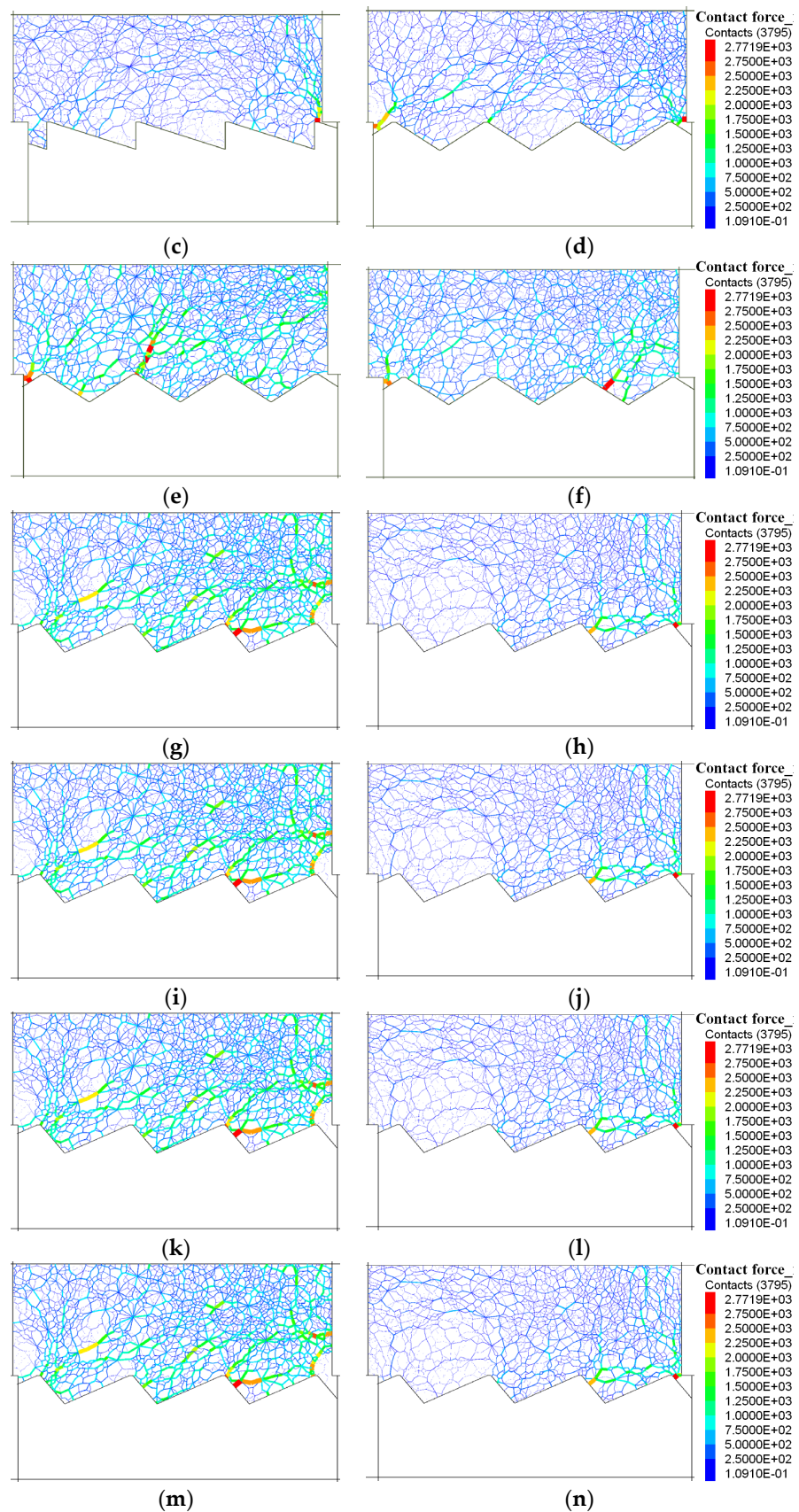


Figure 6. Cont.

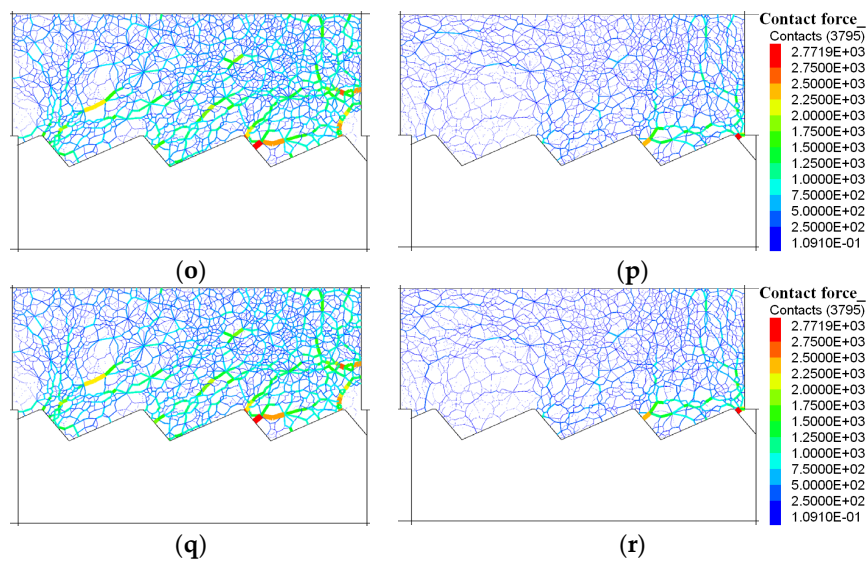


Figure 6. Variation of interparticle contact force with shear displacement at different angles. **(a)** shear displacement = 1 mm, $\theta = 18^\circ$. **(b)** shear displacement = 2 mm, $\theta = 18^\circ$. **(c)** shear displacement = 3 mm, $\theta = 18^\circ$. **(d)** shear displacement = 1 mm, $\theta = 33^\circ$. **(e)** shear displacement = 2 mm, $\theta = 33^\circ$. **(f)** shear displacement = 3 mm, $\theta = 33^\circ$. **(g)** shear displacement = 1 mm, $\theta = 50^\circ$. **(h)** shear displacement = 2 mm, $\theta = 50^\circ$. **(i)** shear displacement = 3 mm, $\theta = 50^\circ$. **(j)** shear displacement = 1 mm, $\theta = 70^\circ$. **(k)** shear displacement = 2 mm, $\theta = 70^\circ$. **(l)** shear displacement = 3 mm, $\theta = 70^\circ$. **(m)** shear displacement = 1 mm, $\theta = 90^\circ$. **(n)** shear displacement = 2 mm, $\theta = 90^\circ$. **(o)** shear displacement = 1 mm, $\theta = 90^\circ$. **(p)** shear displacement = 1 mm, $\theta = \text{random}$. **(q)** shear displacement = 2 mm, $\theta = \text{random}$. **(r)** shear displacement = 3 mm, $\theta = \text{random}$.

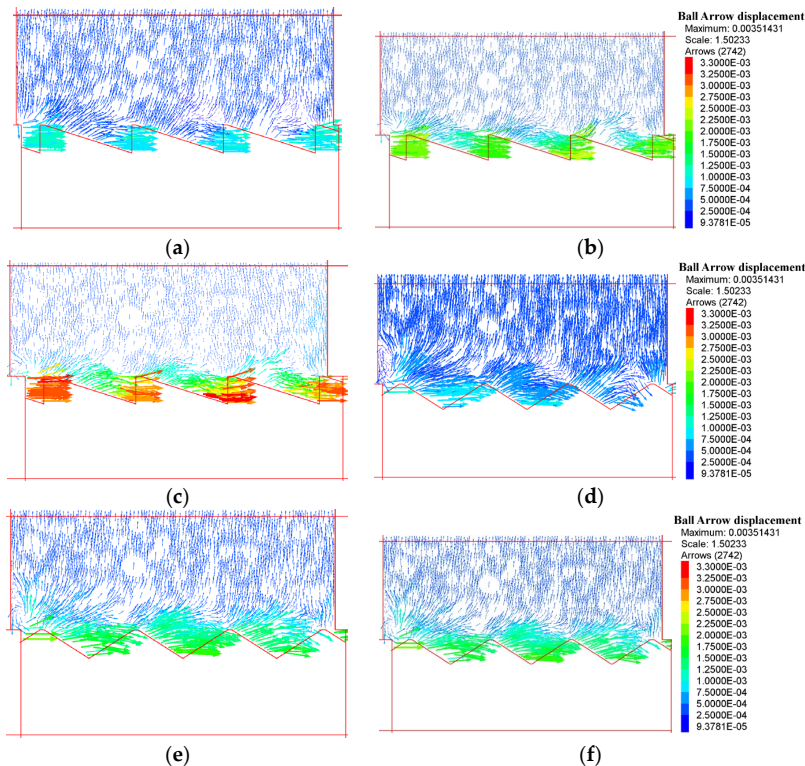


Figure 7. Cont.

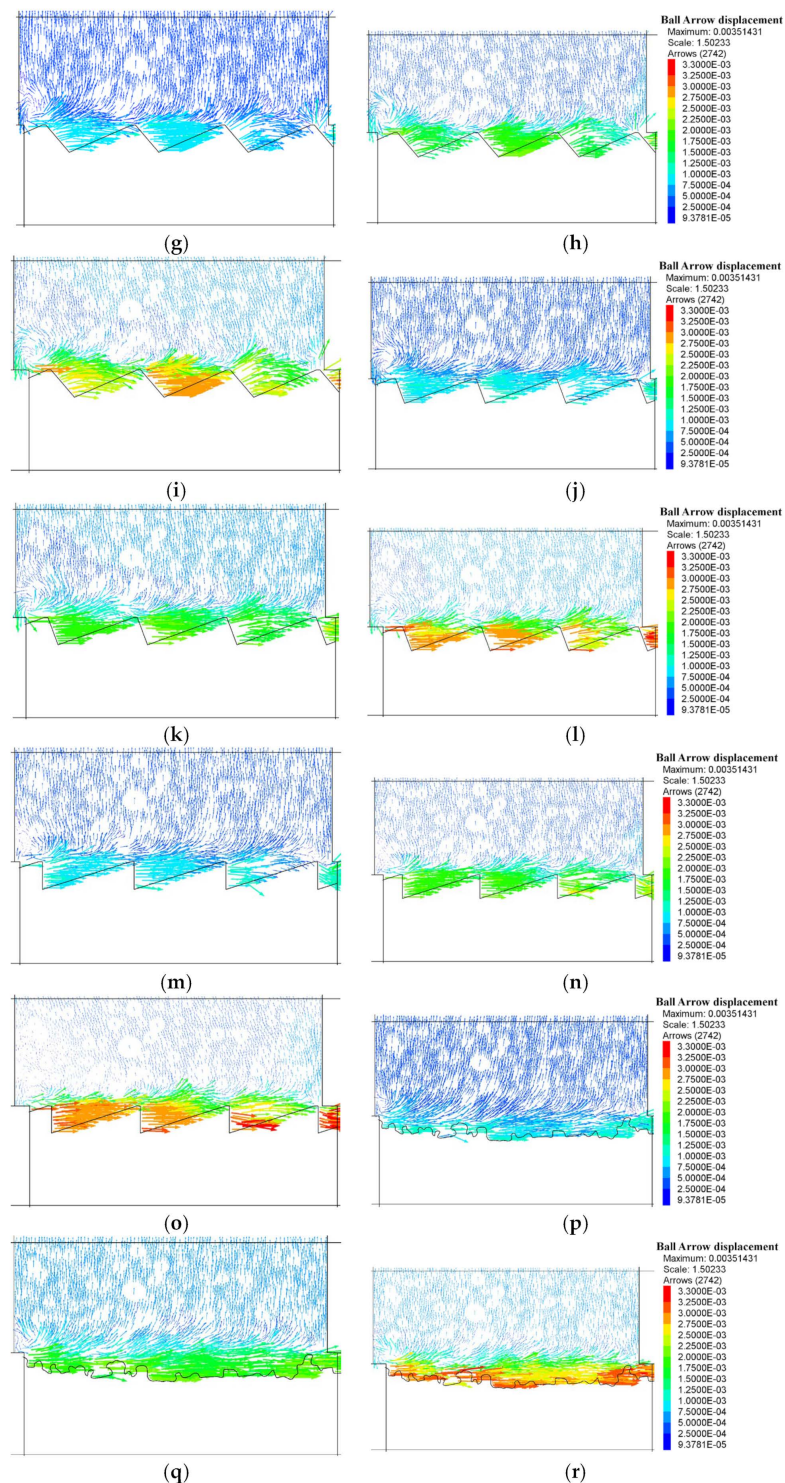


Figure 7. Variation of particle displacement vector with shear displacement. (a) shear displacement = 1 mm, $\theta = 18^\circ$. (b) shear displacement = 2 mm, $\theta = 18^\circ$. (c) shear displacement = 3 mm, $\theta = 18^\circ$. (d) shear displacement = 1 mm, $\theta = 33^\circ$. (e) shear displacement = 2 mm, $\theta = 33^\circ$. (f) shear displacement = 3 mm, $\theta = 33^\circ$. (g) shear displacement = 1 mm, $\theta = 50^\circ$. (h) shear displacement = 2 mm, $\theta = 50^\circ$. (i) shear displacement = 3 mm, $\theta = 50^\circ$. (j) shear displacement = 1 mm, $\theta = 70^\circ$. (k) shear displacement = 2 mm, $\theta = 70^\circ$. (l) shear displacement = 3 mm, $\theta = 70^\circ$. (m) shear displacement = 1 mm, $\theta = 90^\circ$. (n) shear displacement = 2 mm, $\theta = 90^\circ$. (o) shear displacement = 1 mm, $\theta = \text{random}$. (p) shear displacement = 2 mm, $\theta = \text{random}$. (q) shear displacement = 3 mm, $\theta = \text{random}$.

4. Discussion

Sand particle characteristics, the surface features of structures, and test conditions all influence the interface strength. As discovered by J.D. Frost (2002), increased roughness leads to enhanced interlocking between the particles and the structural surface, thereby increasing the shear strength. This paper investigates the effect of changing the angle of triangular protrusions on the shear interface, and finds that, even with the same roughness, the angle of the triangles significantly affects the shear strength. Additionally, increasing the angle also substantially enhances the interlocking effect. The intrinsic laws causing this phenomenon are observed as follows.

The interaction surface, characterized by random and zigzag topography, presents a plethora of interstitial grooves. Throughout the shear, sand particles become embedded within these recesses, navigating them via mechanisms such as sliding, dislocations, and rolling. Within the context of the sawtooth contact interface, at an inclination angle of $\theta = 18^\circ$, the preponderance of sand particles traverses the inclined grooves through processes of sliding and rolling. The distribution of stress across the inclined zigzag surface is significantly heterogeneous, with stress concentration localized at the vertices of the turns. The support stress within the lower mid-plane of the inclined plane is significantly reduced. Sliding, which requires less shear force than climbing or dislocating, dominates as the mode of particle motion. As a result, the shear strength at the contact surface at this specific inclination is observed to be relatively reduced.

At an inclination angle of $\theta = 33^\circ$, particles situated at the base of the grooves face considerable obstacles in surmounting the apices of the sawteeth. Consequently, the preponderance of sand particles traverses the groove through a composite mechanism of rolling, sliding, and dislocations, which precipitates a relatively rapid escalation in the requisite shear force. Between $\theta = 50^\circ$ and $\theta = 70^\circ$, a marked asymmetry in contact force is discerned on the contiguous sides of the sawteeth, with the majority of the contact force being localized to the right side of the sawteeth (oriented towards the direction of displacement). Within this angular range, the dominant mode of particle passage through the sawtooth is dislocations and rolls, which corresponds to a relatively modest enhancement of the shear strength. As the inclination angle extends from $\theta = 70^\circ$ to $\theta = 90^\circ$, a marked surge appeared in the contact force on the left inclined surface of the sawteeth. Particles are dislocated primarily to overcome the sharp corners of the serrations, necessitating a sharp escalation of the shear force. Consequently, the shear strength at the contact surface reaches its maximum at these obliquities.

In summary, increasing the interface roughness is an effective method to improve its shear strength. However, special attention should be paid to the relationship between the regular interface texture (such as the triangular surface studied in this article) and the direction of shearing. When the shear angle is less than 70° , the shear strength will significantly decrease even if the roughness remains unchanged. Currently, factors affecting interface strength have been thoroughly studied, but there are still some practical challenges that need to be addressed. For example, the scale of roughness on structures can span several orders of magnitude, and different roughness ranges can induce different levels of shear strength, which also varies with different particle sizes. Additionally, in DEM numerical simulations, shear strength is quite sensitive to micromechanical parameters such as particle stiffness and the surface stiffness of structures. However, there is still a lack of convenient methods to calibrate the relationship between numerical parameters and physical parameters.

5. Conclusions

The “random type” soil–structure interface shear test was engineered using the sand filling method. Following the identification of the inclination angle range for the triangle contact surface with the most prevalent occurrence, five “regular type” triangle interface direct shear tests were carefully designed with different angles while ensuring the same level of roughness. The PFC2D numerical simulations were employed to examine the

influence of different interfacial configurations on the interfacial shear mechanism. The combined findings are presented below:

- (1) Within the spectrum of different relative densities encountered in sandy soils, shear stress-displacement relations for interfaces exhibiting a variety of morphologies exhibit analogous patterns of behavior. During the application of lower normal stresses (ranging from 50 kPa to 100 kPa), these interfaces demonstrate attributes of ideal elastic–plastic behavior. Conversely, under higher normal stresses (extending from 200 kPa to 300 kPa), a transition towards strain softening is observed. This strain softening is more pronounced at lower relative densities of sandy soils, whereas higher relative densities are associated with a tendency to strain hardening. The shear strength of the random contact interface is positioned at an intermediate level between the shear strengths exhibited by a 70° sawtooth contact interface and a 90° sawtooth contact interface.
- (2) When the angle of the sawtooth is small, the initial shear stage sees the formation of stress concentration around the sawtooth's tip. A stress gap forms between the tips, causing the particle displacement to exhibit a “wave” shape with a peak between the sawteeth. As the angle of the sawtooth increases, the stress on the side of the sawtooth increases, and the stress gap between the sawtooth gradually disappears. As the shear displacement increases, the contact force chain gradually creates an arching effect across several zigzag tips.
- (3) The shear mechanism operates at contact interfaces, which exhibit a diversity of morphological features and exhibit a continuum of behaviors. At a sawtooth angle of 18°, the sand particles predominantly exhibit sliding and rolling motion within the confines of the sawtooth notches. With the increase in sawtooth angle to 33°, the particle interactions transition to include sliding, displacement, and rolling. Within the spectral range of 50° to 70° for sawtooth angles, displacement and rolling emerge as the principal modes of particle transportation through the notches. Notably, at sawtooth angles spanning 50° to 70°, the sand particles primarily undergo displacement within the notches.
- (4) This research results emphasize the significant impact of interface geometry on the shear strength of contact surfaces, providing valuable references for the design and analysis of geotechnical engineering structures such as retaining walls, foundations, or precast piles. This study also reveals some important influencing factors, such as different materials exhibiting different shear characteristics on the same textured interface, including clay, silt, and sands of different gradations. Moreover, experiments at larger scales or in situ conditions have not yet been conducted, so the specific impact of scale effects remains unclear. Additionally, there is currently a lack of a simple and effective method to precisely calibrate the micro parameters of numerical simulations, which limits the accuracy and application scope of numerical simulations.

Author Contributions: Conceptualization, Z.M. and H.L.; methodology, H.L.; software, Z.M.; validation, Z.M., H.L. and Y.L.; formal analysis, Z.M.; writing—original draft preparation, Z.M.; writing—review and editing, Y.L.; visualization, Z.M.; project administration, Z.M.; funding acquisition, Z.M.; Formal analysis, S.S. and H.Z. All authors have read and agreed to the published version of the manuscript.

Funding: This research was funded by the Key Laboratory of Rock Mechanics and Geohazards of Zhejiang Province (No. ZJRMG-2021-05), the Yongjiang Talent Project (No. 2022A-231-G), the General Scientific Research Projects of Zhejiang Education Department (No. Y202249605).

Data Availability Statement: The original contributions presented in the study are included in the article, further inquiries can be directed to the corresponding author.

Conflicts of Interest: Author Songlin Shen was employed by the company China MCC22 Group Corporation Ltd. The remaining authors declare that the research was conducted in the absence of any commercial or financial relationships that could be construed as a potential conflict of interest.

References

1. Zheng, Z.; Naggar, M.H.E.; Wang, J.; Yang, Q. Coupling effect of roughness and normal pressure on mechanical characteristics and failure mode of deep-sea sediment interface. *Ocean Eng.* **2023**, *267*, 113255. [[CrossRef](#)]
2. Hebeler, G.L.; Martinez, A.; Frost, J. Shear zone evolution of granular soils in contact with conventional and textured CPT friction sleeves. *Ksce J. Civ. Eng.* **2016**, *20*, 1267–1282. [[CrossRef](#)]
3. Frost, J.D.; DeJong, J.T. In situ assessment of role of surface roughness on interface response. *J. Geotech. Geoenviron.* **2005**, *131*, 498–511. [[CrossRef](#)]
4. Li, H.H.; Meng, Z.G. Effects of interface morphology on the shear mechanical properties of sand–concrete interfaces. *Materials* **2023**, *16*, 6122. [[CrossRef](#)] [[PubMed](#)]
5. Zhong, W.H.; Liu, H.L.; Wang, Q. Investigation of the penetration characteristics of snake skin-inspired pile using DEM. *Acta Geotech.* **2021**, *16*, 1849–1865. [[CrossRef](#)]
6. Nardelli, A.; Cacciari, P.P.; Futai, M.M. Sand–concrete interface response: The role of surface texture and confinement conditions. *Soils Found.* **2019**, *59*, 1675–1694. [[CrossRef](#)]
7. Xiao, J.; Xu, Z.M.; Wang, L.; Lei, B. Effect of chemical composition of fine aggregate on the frictional behavior of concrete–soil interface under sulfuric acid environment. *Fractal Fract.* **2021**, *6*, 22. [[CrossRef](#)]
8. Martinez, A.; Frost, J.D. The influence of surface roughness form on the strength of sand–structure interfaces. *Geotech. Lett.* **2017**, *7*, 104–111. [[CrossRef](#)]
9. Wang, X.; Wang, X.Z.; Zhu, C.Q.; Meng, Q.S. Shear tests of interfaces between calcareous sand and steel. *Mar. Georesour. Geotech.* **2019**, *37*, 1095–1104. [[CrossRef](#)]
10. Wang, X.; Cheng, H.; Yan, P. The influence of roughness on cyclic and post-cyclic shear behavior of red clay-concrete interface subjected to up to 1000 cycles. *Const. Build. Mater.* **2021**, *273*, 121718. [[CrossRef](#)]
11. Cen, W.J.; Wang, H.; Sun, Y.J.; Wen, L.S. Cyclic behavior of interface shear between carbonate sand and steel. *Acta Geotech.* **2021**, *16*, 189–209.
12. Jin, Z.; Yang, Q.; Chen, C.; Leng, W.; Zhao, C. Experimental study on effects of the roughness on mechanical behaviors of concrete-sand interface. *Chin. J. Rock Mech. Eng.* **2018**, *37*, 754–765.
13. Hu, L.M.; Pu, J.L. Experimental study on mechanical characteristics of soil-structure interface. *Chin. J. Geotech. Eng.* **2001**, *23*, 431–435.
14. Zhang, M.Y.; Bai, X.Y.; Gao, Q.; Wang, Y.H. Laboratory experimental study of pile-soil interface bearing mechanism in cohesive soil. *Rock Soil Mech.* **2017**, *38*, 2167–2174.
15. Mohamad, M.E.; Kueh, A. Friction and cohesion coefficients of composite concrete-to-concrete bond. *Cement Concrete Comp.* **2015**, *56*, 1–14. [[CrossRef](#)]
16. Dove, J.E.; Jarrett, J.B. Behavior of dilative sand interfaces in a geotribology framework. *J. Geotech. Geoenviron.* **2002**, *128*, 25–37. [[CrossRef](#)]
17. O’Hara, K.B.; Martinez, A. Monotonic and cyclic frictional resistance directionality in snakeskin-inspired surfaces and piles. *J. Geotech. Geoenviron. Eng.* **2020**, *146*, 04020116. [[CrossRef](#)]
18. Vangla, P.; Gali, M.L. Shear behavior of sand-smooth geomembrane interfaces through micro-topographical analysis. *Geotext. Geomembr.* **2016**, *44*, 592–603. [[CrossRef](#)]
19. Han, F.; Ganju, E.; Salgado, R.; Prezzi, M. Effects of interface roughness, particle geometry, and gradation on the sand–steel interface friction angle. *J. Geotech. Geoenviron.* **2018**, *144*, 04018096. [[CrossRef](#)]
20. Uesugi, M.; Kishida, H. Frictional resistance at yield between dry sand and mild steel. *Soils Found.* **1986**, *26*, 139–149. [[CrossRef](#)]
21. Imjai, T.; Kefyalew, F.; Aosai, P.; Garcia, R. A new equation to predict the shear strength of recycled aggregate concrete Z push-off specimens. *Cement Concrete Res.* **2023**, *169*, 107181. [[CrossRef](#)]
22. Kefyalew, F.; Imjai, T.; Garcia, R.; Kim, B. Structural and Service Performance of Composite Slabs with High Recycled Aggregate Concrete Contents. *Eng. Sci.* **2023**, *27*, 2024. [[CrossRef](#)]
23. Hu, L.M.; Zhang, B.Y.; Ma, J. Mechanical characteristics for interfaces between granular materials. *Mech. Res. Commun.* **2010**, *37*, 42–46. [[CrossRef](#)]
24. Frost, J.D.; DeJong, J.T.; Recalde, M. Shear failure behavior of granular–continuum interfaces. *Eng. Fract. Mech.* **2002**, *69*, 2029–2048. [[CrossRef](#)]
25. Zhang, N.; Matthew Evans, T. Three dimensional discrete element method simulations of interface shear. *Soils Found.* **2018**, *58*, 941–956. [[CrossRef](#)]
26. GB/T50123-2019; Ministry of Housing and Urban-Rural Development of the People’s Republic of China. Standard for Geotechnical Testing Method. China Planning Press: Beijing, China, 2019.
27. Li, H.H.; Fu, S.J.; Zhu, D.Y.; Li, G.; Shen, S.L. Experimental study on the effects of triangular groove inclination angles on the mechanical behavior of sand–concrete interfaces. *J. Mater. Res. Technol.* **2023**, *24*, 159–172. [[CrossRef](#)]

Disclaimer/Publisher’s Note: The statements, opinions and data contained in all publications are solely those of the individual author(s) and contributor(s) and not of MDPI and/or the editor(s). MDPI and/or the editor(s) disclaim responsibility for any injury to people or property resulting from any ideas, methods, instructions or products referred to in the content.